Transient numerical and physical modelling of temperature profile evolution in stabilised rammed earth walls

M.R. Hall, D. Allinson

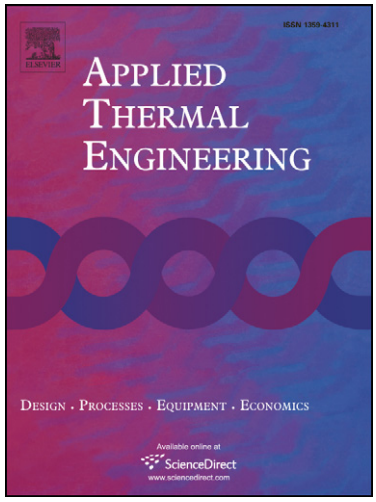

Transient numerical and physical modelling of temperature profile evolution in stabilised rammed earth walls

M.R. Hall, D. Allinson

PII: S1359-4311(09)00294-4
DOI: 10.1016/j.applthermaleng.2009.10.003
Reference: ATE 2899

To appear in: *Applied Thermal Engineering*

Received Date: 15 July 2009
Accepted Date: 5 October 2009

Please cite this article as: M.R. Hall, D. Allinson, Transient numerical and physical modelling of temperature profile evolution in stabilised rammed earth walls, *Applied Thermal Engineering* (2009), doi: 10.1016/j.applthermaleng.2009.10.003

Transient numerical and physical modelling of temperature profile evolution in stabilised rammed earth walls

M R Hall [a]* **and D Allinson** [b]

[a] *Faculty of Engineering, Department of the Built Environment, University of Nottingham, University Park, Nottingham NG7 2RD, UK Tel: +44 (0) 115 846 7873, Fax: +44 (0) 115 951 3159, E-mail: matthew.hall@nottingham.ac.uk*

[b] *Department of Civil & Building Engineering, Loughborough University*

*corresponding author

Abstract

Three established stabilised rammed earth (SRE) mix types (433, 613, 703) were identified for analysis, in the form of 300mm thick test walls, by being subjected to different static air temperature and relative humidity differentials. The predictive numerical model outputs from WUFI Pro v4.1 hygrothermal simulations displayed good accuracy when validated against experimental data from physical modelling conducted using test walls in a climatic simulation chamber. The wall temperature profile evolution and resultant steady state gradients were very similar regardless of mix type indicating that the majority of the wall remained relatively dry. Unless liquid water is present, the thermal resistance and heat capacity of these materials does not change sufficiently to make significant differences to temperature profile evolution regardless of soil mix type. Little scope exists to intelligently modify the ability of SRE walls to absorb and store heat energy simply by manipulation of particle size distribution (PSD) and the resultant bulk density/void ratio relationships, under these conditions. Only the outer layers of the walls appear to interact with moisture in the air, and the predicted transient responses indicate that significant potential exists to

intelligently modify the ability of SRE walls to absorb, store and release moisture vapour from the surrounding air simply by manipulation of PSD and the resultant bulk density/void ratio relationships.

Keywords: transient thermal modelling; stabilised rammed earth; hygrothermal properties; climatic simulation chamber, temperature buffering; WUFI

Nomenclature

D_φ	liquid conduction coefficient
H	enthalpy (J)
H_{vap}	enthalpy of vaporisation (J)
p_{sat}	saturation vapour pressure (Pa)
t	time (s)
T	temperature (°C)
w	specific moisture content (kg/m^3)
φ	relative humidity (decimal)
λ	thermal conductivity (W/m K)
δ_p	water vapour permeability (kg/m s Pa)

1. Introduction

SRE (soil-based) materials have a good potential to buffer air temperature and relative humidity fluctuations in response to climatic variables in a controlled environment, e.g. inside an occupied building, industrial premises, or for the archiving/storage of sensitive media [1, 2]. The passive buffering of relative humidity inside earth buildings has been reported [3] and the role of other absorbent building materials measured [4, 5]. It is hypothesised that the

functional properties controlling this behaviour are a product of controllable material characteristics in earth materials and that these can be optimised to suit the application. In order to begin to understand this requires a transient hygrothermal approach for predictive numerical modelling, which therefore requires validation by coupled physical modelling. One must consider both the climatic conditions and the material properties, both of which dynamically change as a function of time.

The authors have previously shown that whilst the dry-state thermal conductivity for compacted earth material types appears to vary little, their moisture-dependent thermal conductivity varies significantly due to the wide range of possible internal pore structures. As a result, the moisture-dependent volumetric heat capacity can experience even greater fluctuations [1, 6]. The authors have also previously found that (by analogy) the reverse is true for moisture, where the sorption isotherms between possible SRE types varies little, but that liquid water sorptivity/desorptivity, and also water vapour permeability, can vary over a significantly large range. Since temperature gradients induce mass transfer inside the material, and the thermal properties are moisture content-dependent, one can appreciate the fully transient nature of the coupled heat & mass transport phenomena associated with material behaviour in relation to air temperature and relative humidity buffering. The diagram in figure 1 illustrates hygrothermal behaviour in relation to the wall of a building [7]. In addition, phase change of moisture transporting within the material has to be considered in relation to the heat flux associated with its enthalpy of vaporisation.

This paper describes how a transient hygrothermal numerical model was used to simulate the behaviour of walls, made from three contrasting SRE material types, in response to changes in adjacent environmental conditions. These simulations were replicated as a full-scale physical model by constructing the said walls in a climatic simulation chamber and imposing realistic

78 indoor/outdoor environments either side of the walls. The objective of the modelling exercises
79 was to validate the numerical predictions for temperature profile evolution by assessing the
80 hygrothermal behaviour of the materials.
81
82 **2. Transient numerical modelling of heat & mass transport/storage**
83 When considering simultaneous transient modelling of heat & mass transport/storage in
84 porous media the thermodynamic behaviour is referred to as hygrothermal. Transient
85 hygrothermal simulation tools include the following transport and storage phenomena:
86
87 • heat storage in dry, unsaturated and saturated porous media
88 • dry and moisture-dependent thermal conductivity (heat transport)
89 • latent heat transport as a result of vapour diffusion (including phase change due
90 to vapour evaporation/condensation)
91 • water (mass) storage by water vapour sorption and liquid capillarity
92 • water vapour transport by diffusion
93 • liquid transport by surface diffusion and capillary conduction
94
95 Numerous models exist for the definition of these phenomena (see [8] for a good summary).
96 Note that the benchmark standard BS EN 15026:2007 assumes that there is no total pressure
97 difference across the component under consideration and air movement is ignored [9]. The
98 well-established WUFI® model [10, 11] uses two coupled equations; one for heat transport
99 (Eq 1) and the other for mass transport (Eq 2). They are solved simultaneously and
100 numerically using an implicit finite volume method of discretisation with a tridiagonal matrix
101 algorithm (known as the Thomas algorithm).
102

$$\frac{\partial w}{\partial \varphi} \cdot \frac{\partial \varphi}{\partial t} = \nabla \cdot \left(D_\varphi \nabla \varphi + \delta_p \nabla (\varphi \, p_{sat}) \right) \quad \text{(Eq. 1)}$$

$$\frac{\partial \mathrm{H}}{\partial T} \cdot \frac{\partial T}{\partial t} = \nabla \cdot (\lambda \nabla T) + \mathrm{H}_{\mathrm{vap}} \nabla \cdot \left(\delta_p \nabla (\varphi \, p_{sat}) \right) \quad \text{(Eq. 2)}$$

In equation 1, the left side of the moisture balance terms represents water storage which is proportional to the derivative of the water retention curve ($\partial w/\partial \varphi$), i.e. defined by the sorption isotherm. The divergence of liquid and vapour flow is computed using the transport terms on the right side of equation 1. The partial vapour pressure differential is the motivational force for vapour diffusion, and is strongly temperature dependent since $p_{sat} \approx \exp(T)$. Liquid flow, on the other hand, is dominated by capillary forces which are chiefly a function of relative humidity φ (Kelvin equation). Note that the WUFI model ignores the influence of temperature on capillary-induced liquid flow. In equation 2, the sensible heat flow is simply represented by the divergence of heat conduction, whilst the divergence of vapour flow multiplied by the enthalpy of vaporisation represents the latent heat term on the right hand side. The derivative of total enthalpy, on the left hand side of equation 2, represents energy storage and contains the heat capacity of the dry material plus the enthalpy of absorbed water, which is itself phase-dependent (i.e. solid, liquid or vapour).

The hygrothermal material properties for each of the three SRE material types are taken from published data by the authors [1] and were used as the input parameters for the WUFI Pro simulations. As with most porous civil engineering materials (e.g. concrete, brick, soil) SRE is not homogenous because the pore size distribution and tortuosity vary greatly within the material. The conventional, accepted approach to measuring coefficients related to transport processes is to test a representative sample of the material and use this output as the volume averaged coefficient for that material, e.g. thermal conductivity. Obviously, no one individual

part of the material has this property because it has effectively been statistically weighted, but across a representative area at full scale it is valid. The higher the sample population during testing, the greater the accuracy of the mean value. The required number of samples needed to achieve this, as detailed in the relevant BS EN ISO standards, was used for the testing conducted by the authors for this work [15].

Both in the numerical model (WUFI Pro) and the physical model (climate chamber tests), the indoor and outdoor initial conditions for the simulation were taken as 21°C and 45% relative humidity. At time, $t = 0$ the outside climatic set points were adjusted to 8°C and 70% RH. Further set point changes were introduced at 48 hours and 72 hours, when temperatures were reduced to 0°C and -8°C respectively whilst maintaining a constant 70% RH. The simulations ran for a total of 96 hours. The surface resistances for heat transfer and vapour diffusion were given typical values of 0.125m^2 K/W and 45.45x10^6 m^2 s Pa/kg respectively. These values were the same for both sides of the test walls to suit the conditions found in the climatic simulation chamber experiments.

3. Physical modelling in the climatic simulation chamber

The simulation chamber itself is composed of two self-contained halves called the 'design' side and the 'climate side' that join together on either side of the test specimen. The dimensions of each chamber are 4m long, 3m wide and 2.6m in height. The normal operating temperature range is +20°C to −15°C (± 5°C) depending on the internal conditions specified [12]. A schematic diagram illustrating the basic operation of the climatic simulation chamber is shown in Figure 2. Full-scale test components (e.g. walls) can be constructed inside the climatic simulation chamber following normal construction practices, and realistic climatic effects (on both sides of the walls) including various weather conditions can be accurately simulated and monitored under controlled laboratory conditions [13, 14]. The design side of

154 the simulation chamber represents the interior conditions of a building and is typically
155 configured to maintain standard indoor room conditions of 20°C ±1° and 45% RH ±5%. The
156 climate side of the simulation chamber creates realistic sequences of different external
157 weather conditions that can run in a fixed mode, sequence mode, or cyclic mode. The
158 advantage of this is that the start and finish temperatures can be specified, as well as the rates
159 of change of other weather components such as air pressure, relative humidity and rainfall.
160
161 The 300mm-thick SRE test walls were constructed inside the climatic simulation chamber on
162 top of a concrete plinth, as described in previous work published by Hall [14]. The walls were
163 made using the 433, 613 and 703 mix types detailed in previous studies [1, 6, 14, 15]. The
164 aggregates and silty clay, along with the mix types, were specified and controlled to be
165 precisely the same as those used for the small representative test specimens. Prior to
166 compaction the soils were mixed to their optimum moisture content and placed in layers
167 150mm thick inside oiled proprietary formwork and compacted using an Atlas Copco RAM30
168 pneumatic tamper. The test walls were separated from one another by a 100mm thick timber-
169 frame incorporating the formwork end boards. Following their completion, the test walls were
170 allowed to cure for a minimum period of 28 days in laboratory conditions at 22°C ±1° and
171 40% RH ±5%. The wall edges were sealed with phenolic resin-coated plywood and caulked
172 with silicone sealant. The remaining height above the test walls was completed with timber
173 frame walling and covered with 1200g damp proof membrane sealed with black cloth tape.
174 The resultant dimensions for the exposed test face of each wall were 500mm wide by 900mm
175 high (area = 0.45m^2).
176
177 An array of electronic sensors was retrofitted to each of the four rammed earth test walls by
178 drilling a small hole from the inside of the wall to the required depth and then carefully
179 inserting the sensor using metal rod marked at different depths. Once in place the sensor hole

was capped and sealed using silicone caulking. In each wall, six type-T copper/constantan thermocouples (protected by hollow plastic tubing) were installed to depths of 25mm, 50mm, 75mm, 100mm, 125mm, and 150mm. In addition, armoured thermocouples were mounted onto both the internal and external wall faces.

The simulation parameters involved creating various fixed temperature & humidity gradients across the test walls. This was achieved in the climate chamber by maintaining a difference in temperature/humidity between the design side and the climate side of the chamber for a 24-hour period. All of this testing was performed in the absence of any rainfall or pressure differential. The indoor (design side) conditions were maintained at 20°C ±1° and 40% RH ±5% to represent a comfortable indoor living environment. The outdoor conditions (climate side) were kept at a constantly high level of relative humidity: 75% ±5% to represent a damp, temperate climate. The test run lasted for a total period of four days and included three different outdoor temperature set points. On days 1 and 2 the 'outdoor' conditions were set to 8°C 75% RH, on day 3 they were set to 0°C 75% RH, and on day 4 they were set to -8°C 75% RH, during which snowfall began to occur. During all four days of the test run the sensor array was used for recording the performance of the test walls.

4. Analysis of simulated temperature and moisture profile evolution

The predictive numerical model outputs from WUFI Pro simulations were compared with experimental data from the physical model using the climatic simulation chamber. The temperature of the inside surface, mid-point and outside surface of each wall are plotted against elapsed time in Figures 3, 4 and 5, for each of the test walls. It can be seen that the simulation mainly predicts the temperatures to a good level of accuracy in relation to the recorded data from the climatic simulation tests.

206 The temperature profile evolution, as a function of time, was calculated for the three walls and
207 representative values at 0, 2, 6, 12, 24, 48, 72 and 96 hours were plotted on the graphs in
208 Figures 6, 7, and 8. It is notable that the temperature profiles do not become linear (i.e.
209 apparent steady state conditions) until around 48 hours after the first temperature set points
210 were initiated, and then at 72 and 96 hours respectively in response to the second and third
211 temperature set point initiations. This enforces the important point that steady state heat loss
212 assumptions are (in the absence of static temperature gradients) inappropriate for simulating
213 the thermal behaviour under the varying environmental conditions that occur in nature. The
214 small variations in volumetric heat capacity of the three soil mix types tested here appeared to
215 make little difference to the time-dependent evolution of the apparent steady state temperature
216 profiles. This suggests that little scope exists to intelligently modify the ability of SRE walls
217 to absorb and store heat energy simply by manipulation of PSD and the resultant bulk
218 density/void ratio relationships.
219
220 The apparent steady state temperature depth profiles appeared to be remarkably similar to one
221 another for each soil mix type. This is consistent with previous findings for dry-state thermal
222 conductivity on these soil mix types [1], and hence the thermal resistance of each wall is very
223 similar indicating that the majority of the wall remained relatively dry. The presence of
224 significant quantities capillary-domain water can cause large increases in the thermal
225 conductivity of the material, which is significantly different between soil mix types according
226 to their void characteristics.
227
228 The change across three external climate set points (8° C 75% RH; 0° C 75% RH; and - 8° C
229 75% RH) presented a situation where the partial vapour pressure, and hence absolute moisture
230 content, of the air on one side of the walls was significantly reduced in each case, as
231 illustrated by the psychrometric chart in Figure 9. Figures 10, 11 and 12 show the transient

simulation results for relative humidity (of the internal pore structure) and moisture content of each test wall at 48, 72 and 96 hour increments. It is apparent that only the internal and external outer layers (approx. 5cm thick) were involved in the interaction with changing humidity over a daily period. One can appreciate the drying appears to occur on the external side when the temperature (and hence the air moisture content at 75% RH) is sufficiently low, and the absorption that occurs on the internal side as a result of the vapour pressure differential across the wall. Interestingly, there appears to be a large disparity between the three soil mix types in terms of i) the mass of absorbed water in the wall core, and ii) the rate of change in moisture content and relative humidity in the outer wall layers. This suggests that significant potential exists to intelligently modify the ability of SRE walls to absorb, store and release moisture vapour from the surrounding air simply by manipulation of PSD and the resultant bulk density/void ratio relationships. This merits further investigation into optimisation of the moisture buffering capacity of SRE materials and possible applications.

Some small discrepancies appeared between numerically and physically modelled temperature data, which could be explained by a number of specific issues. Due to a brief start up period prior to the beginning of the climate chamber simulations, a gradual decrease in the outside wall surface temperatures had already begun whereas for the computer simulation an instantaneous temperature drop from 21°C to 8°C was assumed. The climate side and design side air temperatures within the simulation chamber were not steady state throughout the test period, reflected by the small periodic fluctuation in the recorded wall surface temperatures (i.e. on/off cycling of the control plant). Also, some temperature stratification could reasonably be expected due to imperfect mixing of the air in the chamber and the induced temperature step changes did not occur instantaneously, as they did in the model.

Previous research found that the macro-scale properties of dry density and porosity of large scale SRE test walls could be matched very closely to small Proctor test specimens by accurately controlling PSD and optimum moisture content, regardless of varying compaction input energy. However, other scale effects such as surface finish, compaction layer thickness and degree of homogeneity could reasonably cause disparity between functional hygrothermal properties of the SRE test walls compared to the 1 litre test specimens used to determine the input parameters for the WUFI Pro simulations. Whilst the degree of accuracy in hygrothermally modelling temperature profiles in SRE materials is acceptably accurate, the opportunities for further improvements outlined above require much further research.

5. Conclusions

The numerically modelled data from WUFI Pro v4.1 has been validated to a good level accuracy against the physically modelled experimental data from the climatic simulation chamber. Experimentally determined hygrothermal properties for SRE materials can be inputted to WUFI Pro and used to accurately simulate transient behaviour of full sized test walls in response to changes in climatic conditions as a function of time.

The temperature profile evolution and resultant steady state gradients, in each test wall, were very similar regardless of soil mix type indicating that the majority of the wall remained relatively dry. This is further supported by the predicted liquid and relative humidity content and distribution within each test wall. From previous research [1, 6] it is known that unless liquid water is present, the thermal resistance and volumetric heat capacity of these materials does not change sufficiently to make significant differences to temperature profile evolution regardless of soil mix type. Therefore, there appears to be little scope to intelligently modify the ability of SRE walls to absorb and store heat energy simply by manipulation of PSD and the resultant bulk density/void ratio relationships, under these conditions.

Only the outer layers of the walls appear to interact with moisture in the air. The predicted transient response of material moisture content indicate that significant potential exists to intelligently modify the ability of SRE walls to absorb, store and release moisture vapour from the surrounding air simply by manipulation of PSD and the resultant bulk density/void ratio relationships. The WUFI Pro model appears to show that the relationship between thermal and hygric (hygrothermal) functional properties must be simultaneously balanced in order to control the moisture sorption/desorption rates and storage capacity that govern air temperature and relative humidity buffering. Future research must attempt to scale up the simulation so that whole building modelling and real weather data can be included, and seasonal or annual timeframes can be modelled. Liquid water transport will also be studied so that rain fall absorption can be simulated, which will necessitate modelling over periods of many months. The potential of SRE walls to offer improved thermal comfort and operational energy savings from air conditioning inside buildings is still to be quantified. This work has identified the use of a hygrothermal approach to tackle this problem and has proven that data from numerical and physical models can be accurately validated under controlled climatic scenarios.

Acknowledgements

The authors wish to acknowledge the support of the Engineering and Physical Sciences Research Council for the research presented in this paper.

References

1. Hall M and Allinson D, 2009, 'Analysis of the Hygrothermal Functional Properties of Stabilised Rammed Earth Materials', *Building and Environment* 44 [9] pp. 1935 – 1942

2. Houben H & Guillaud H, 1994, *Earth construction: a comprehensive guide- Reissue edition,* ITDG Publishing, London
3. Minke G, 2000, *The Earth Construction Handbook*, WIT Press, UK
4. Padfield T, 1998, *The role of absorbent building materials in moderating changes of relative humidity*, PhD thesis, The Technical University of Denmark
5. Olaken O & Simonson C, 2006, 'Moisture buffering capacity of hygroscopic building materials: experimental facilities and energy impact', *Energy and Buildings* 38 [10] pp. 1270-1282
6. Hall M & Allinson D, 2008, 'Assessing the moisture-content dependent parameters of stabilised earth materials using the cyclic-response admittance method', *Energy and Buildings,* 40 [11] pp. 2044-2051
7. ASHRAE, 2009, *Handbook of Fundamentals: Chapter 25 - heat, air and moisture control in building assemblies – fundamentals*, ASHRAE, USA
8. Hens H, 1996, 'Heat, Air and Moisture Transfer in Insulated Envelope Parts, Modelling, Common Exercises', *IEA-exco ECBCS,* Annex 24 Final Report – Vol. 1, Addendum, Acco, Leuven
9. BSI, 2007, *BS EN 15026:2007 Hygrothermal performance of building components and building elements- Assessment of moisture transfer by numerical simulation*, British Standards Institute, London
10. Künzel HM, 1995, 'Simultaneous Heat and Moisture Transport in Building Components - One- and two-dimensional calculation using simple parameters', IBP Fraunhofer, Germany. Available http://publica.fraunhofer.de/eprints/urn:nbn:de:0011-px-566563.pdf
11. Karagiozis AN, 2001, 'Advanced Hygrothermal Models and Design Models', in the proceedings for the *Canadian Conference on Building Simulation*, Ottawa, International Building Performance Simulation Association (IBPSA), pp. 547 – 554, June 13 – 14

12. Taylor-Firth A & Flatt DE, 2001, 'Climatic Simulation and Environmental Monitoring - A Facility for Realistic Assessment of Construction Materials In-Service Performance', *Construction & Building Materials*, 5 [1] pp. 3-7

13. Laycock EA, Hetherington S & Hall M. 2002. *Damp Towers - Understanding and Controlling the Ingress of Driven Rain through Exposed Solid Masonry Wall Structures.* Confidential report for English Heritage, London

14. Hall M, 2007, 'Assessing the Environmental Performance of Stabilised Rammed Earth Walls using a Climatic Simulation Chamber', *Building and Environment,* 42 [1] pp.139-145

15. Hall M & Djerbib Y, 2004, 'Rammed earth sample production: context, recommendations and consistency', *Construction and Building Materials*, 18 [4] pp.281-286

345 **Figure Captions**

366

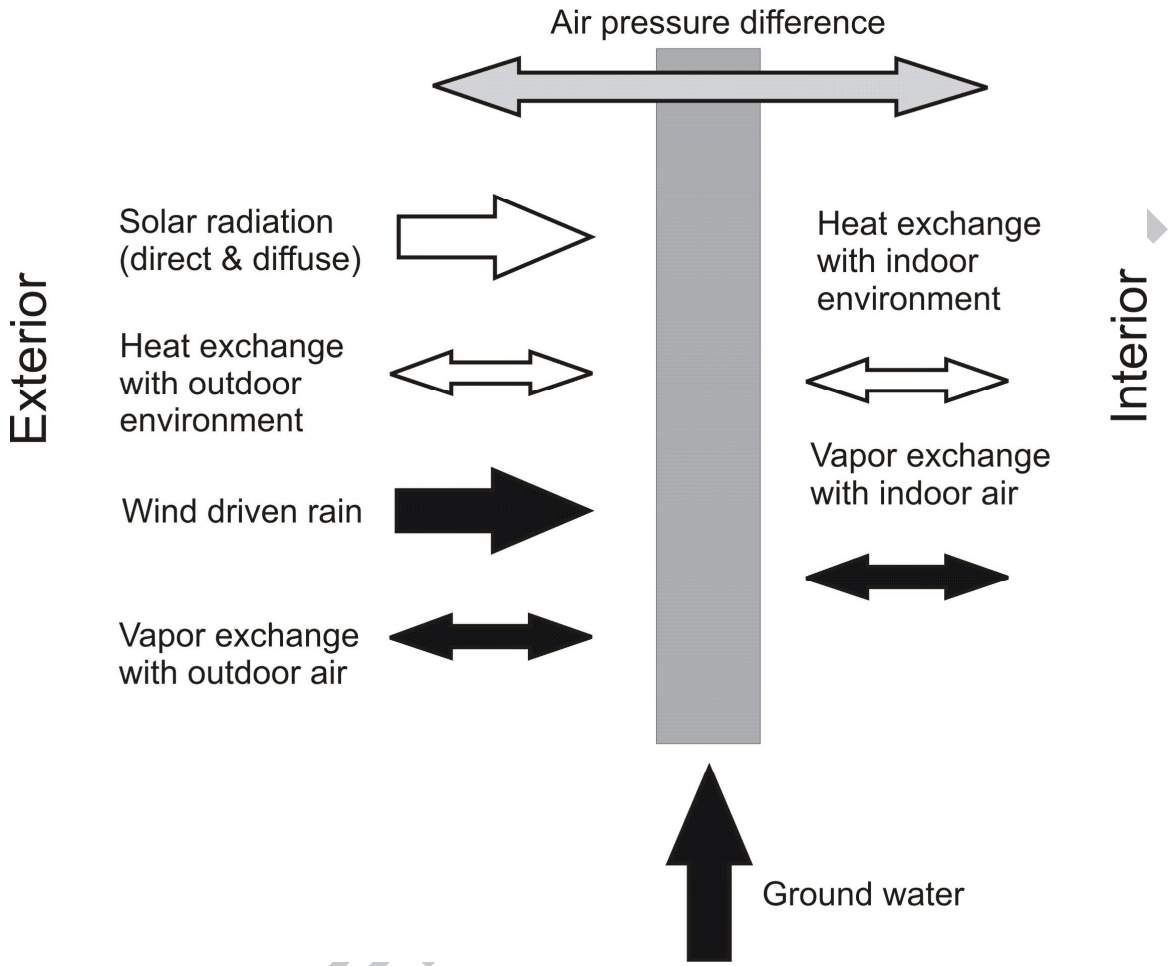

367

368

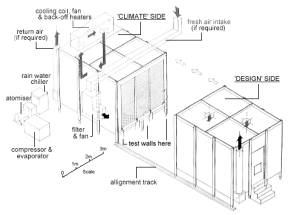

369

370

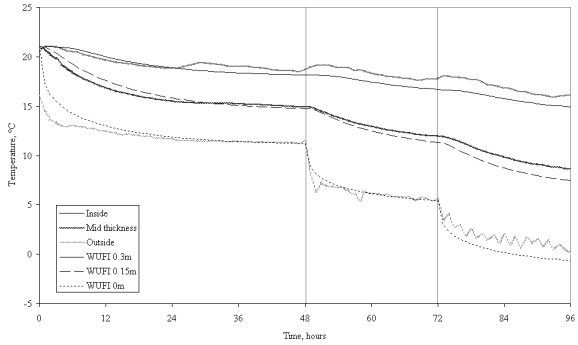

371

372

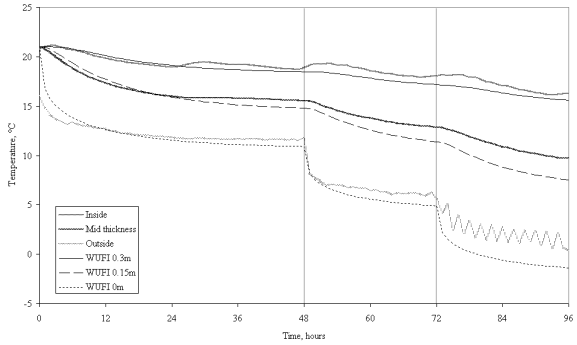

373

374

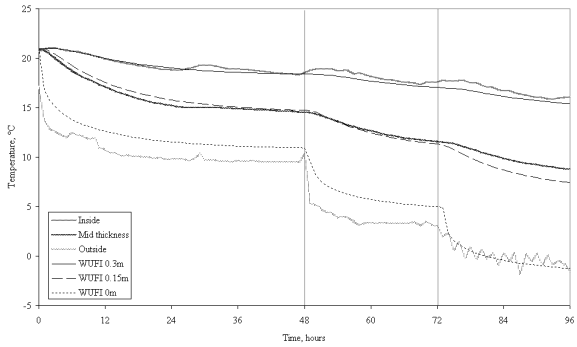

375

376

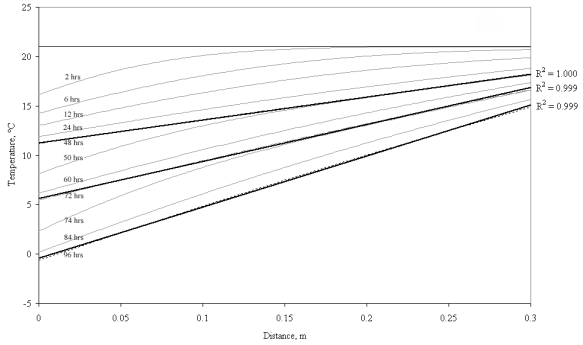

377

378

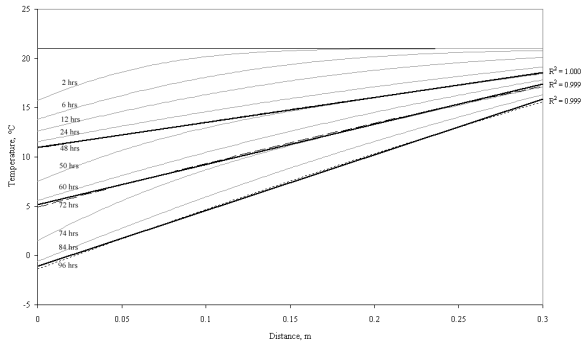

379

380

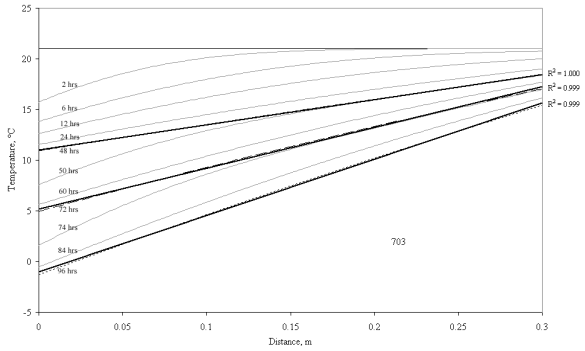

381

382

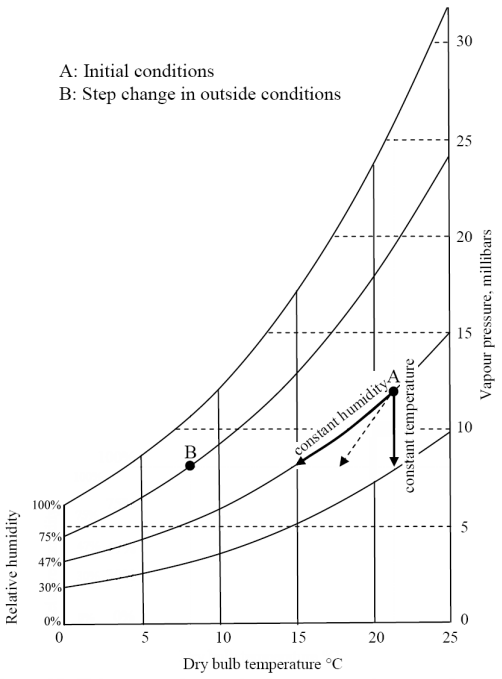

383

384

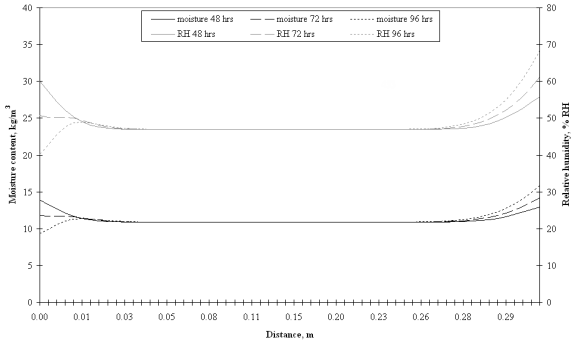

385

386

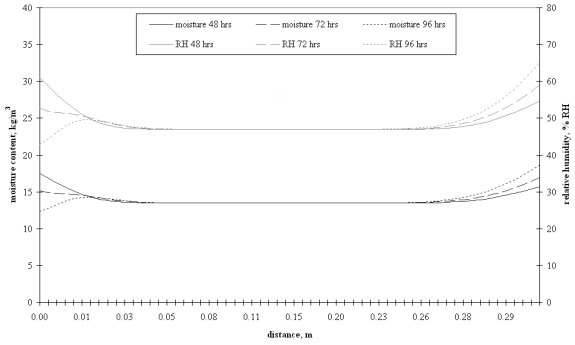

387

388

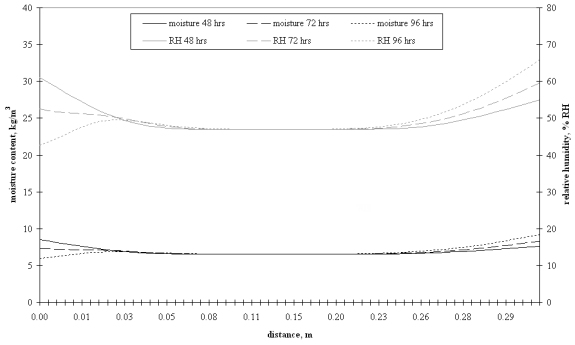

389

390

391 Figure 2

392

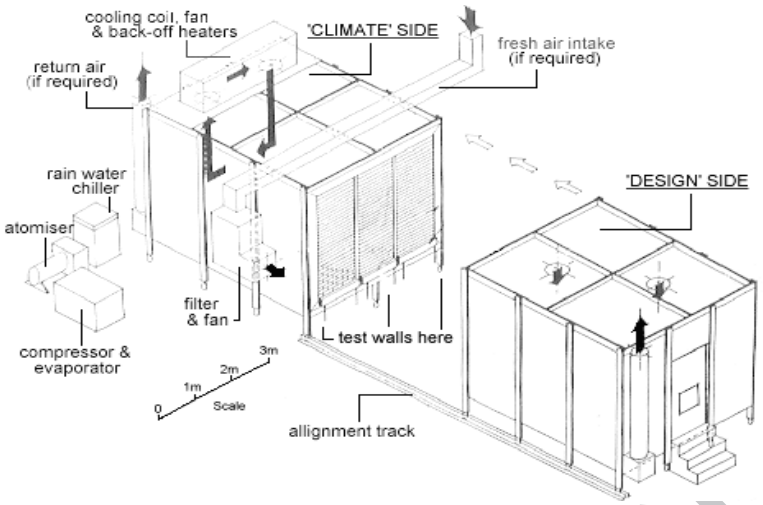

393

394

395

396

397

398

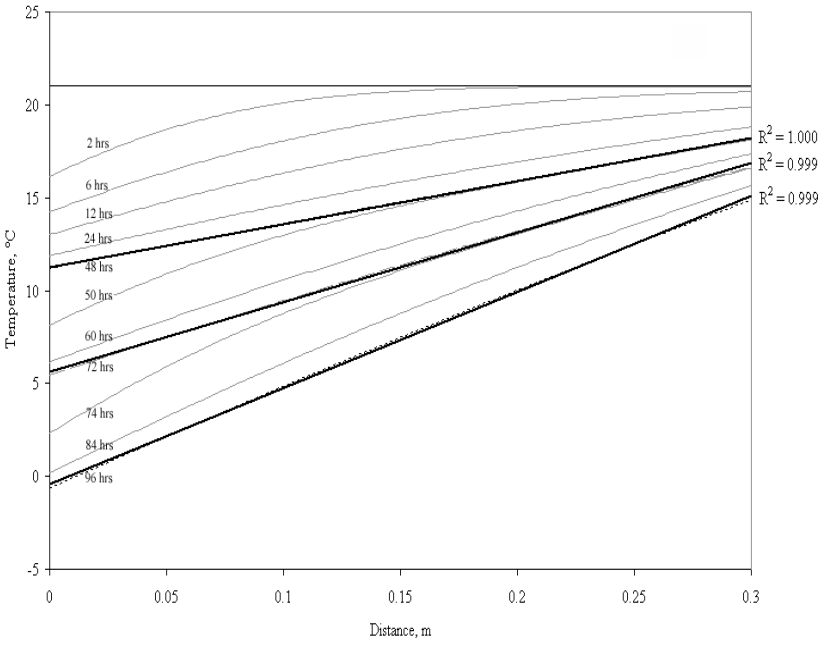

399

400

401

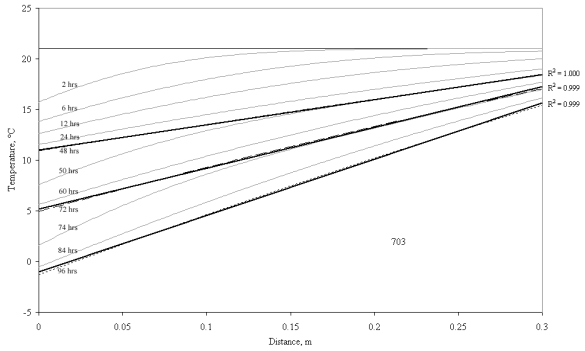

402

Figure 2

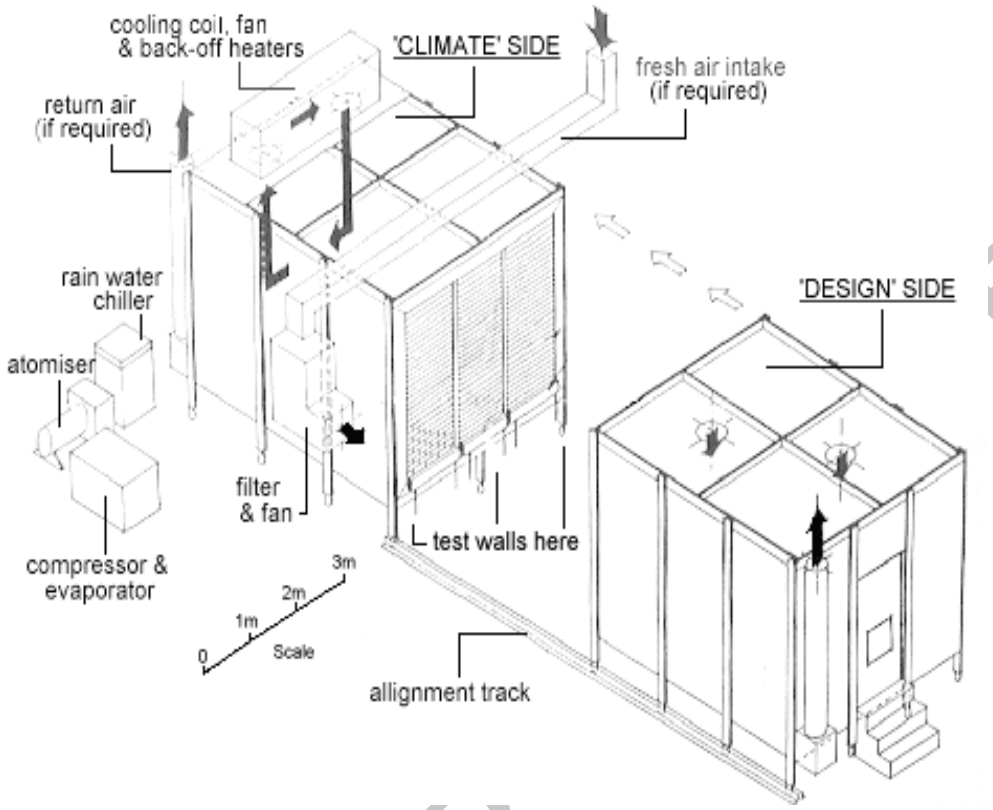

Figure 6

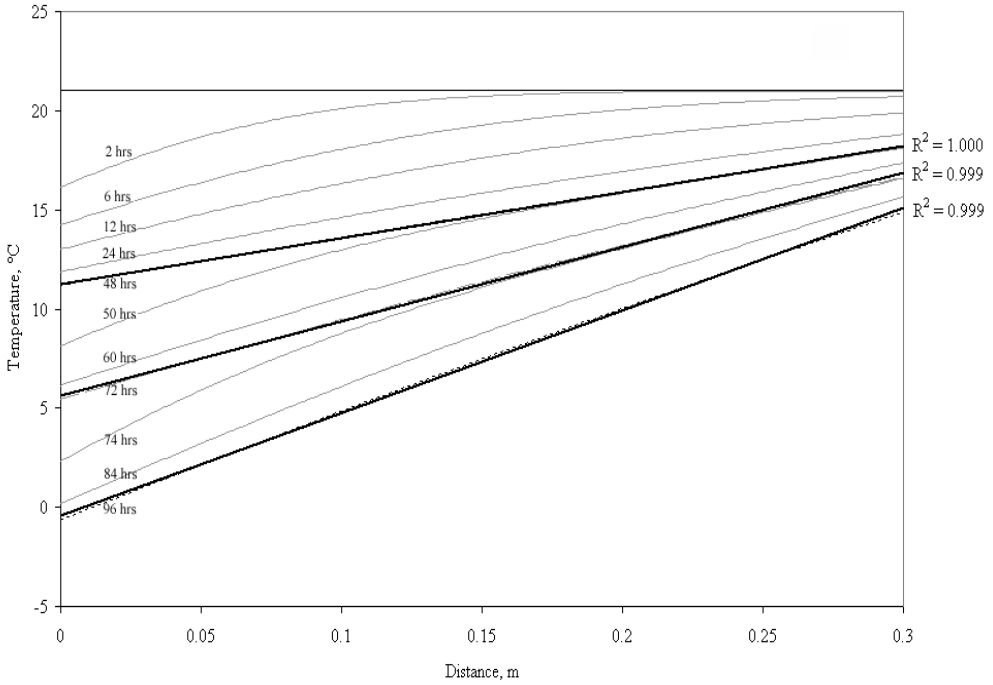

Figure 7

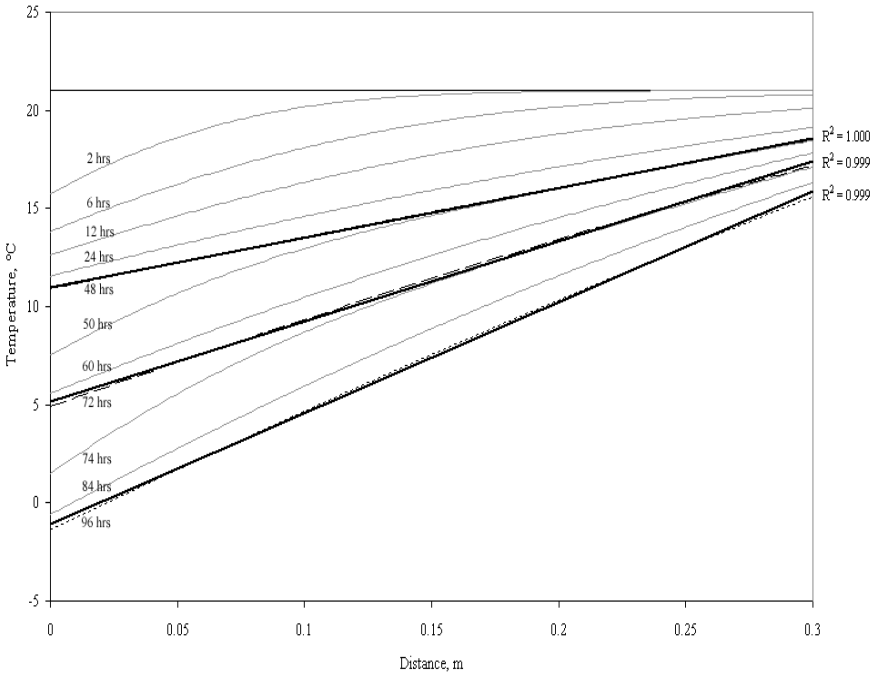

Figure 8